Temperature-driven BCS-BEC crossover and Cooper-paired metallic phase in coupled boson-fermion systems

Maciej M. Maśka[*]
Department of Theoretical of Physics, Wrocław University of Science and Technology, Wybrzeże Wyspiańskiego 27, 50-370 Wrocław, Poland

Nandini Trivedi[†]
Department of Physics, The Ohio State University, 191 West Woodruff Avenue, Columbus, Ohio 43210, USA

(Received 5 April 2018; revised 1 September 2020; accepted 21 September 2020; published 8 October 2020)

Motivated by strongly correlated and frustrated systems, we propose an effective model that describes the dynamics of pairs of opposite spin fermions scattering from localized bosons. Integrating out one of the degrees, either the bosons or fermions, generates temperature-dependent long-range effective interactions between the entities that we investigate using Monte Carlo techniques. The behavior of bosons is dominated by vortex-antivortex unbinding, with effective interboson interactions beyond the nearest-neighbor Josephson coupling of phases. Remarkably, in the fermion sector we observe a temperature-driven phase transition from a SC phase with a "BCS" spectral function that shows a gap minimum on the underlying Fermi surface to a conducting phase of pairs but with a "BEC" spectral function with a gap minimum at $k = 0$. Tunneling and angle-resolved photoemission spectroscopy on Bose-Fermi mixtures in cold atomic systems and superconducting islands on graphene are some of the promising experimental platforms to test our predictions.

DOI: 10.1103/PhysRevB.102.144506

I. INTRODUCTION

Strongly interacting systems lead to emergent phases with spontaneously broken symmetries, such as magnets with broken time-reversal symmetry and superconductors with broken gauge symmetry. Even within the superconducting phase, the system can show effects of interactions evolving from a BCS regime with large Cooper pairs compared to interparticle spacing to a strongly coupled regime where the Cooper pairs are tightly bound [1]. Such an evolution of a system from a BCS to a BEC regime has been predicted as a function of increasing pairing interaction and observed in experiments [2–4]. In this paper, we discover a phase transition at T_c from the SC state in which the single-particle spectrum has a "BCS" character with a minimum gap contour on the underlying Fermi surface, to a high-temperature state where phase fluctuations destroy long-range phase coherence but not pairing and yields a spectral function of "BEC" character with a gap minimum at $k = 0$. Furthermore, the pairs are conducting, yielding a metallic state of pairs, dubbed the Cooper pair metal. In this prediction, a Cooper pair metal originates from an explicit calculation of a model.

Another important feature captured by our model is that even in weak coupling when the spectral gap is "BCS"-like, with increasing temperatures the gap does not close at T_c as expected within BCS theory; instead the gap fills up. Such behavior has been observed in experiments on strongly correlated superconductors. We can now identify the origin of such behavior as arising when phase fluctuations are the route to destruction of superconductivity. The model we consider has noninteracting spin-full fermions that interact with localized bosons. The only interactions are local and occur between two fermions of opposite spin and a boson, illustrated in Fig. 1.

The original motivation for the model comes from recognizing that strongly interacting systems, such as fractional quantum Hall effect, frustrated magnets, and high-T_c superconductors, can be described in terms of emergent degrees of freedom that interact via fluctuating gauge fields. In high-temperature superconductors, for example, strong on-site Mott interactions generate effectively a two-component system in which the fermionic holes become superconducting in a matrix of bosonic fluctuations of the spin singlets. While many issues are still hotly debated, such as the role of intertwined order [5], it is nevertheless remarkable that the broad phenomenology can be understood in terms of a two-component response with the hole density determining the superconducting transition temperature T_c, and the spin singlets generating the pseudogap scale T^* below which a soft gap opens up in the density of states [6]. The effective approach that we discuss below is an attempt to capture the dynamics of such emergent two-component systems in strongly interacting systems.

Another broad class of problems that the model we study pertains to is the superconductor-insulator transition in disordered films, where the possibility of an intervening Bose metallic phase is hotly debated. Our results show that a Bose metal phase at finite temperatures can arise due to classical phase fluctuations. It is possible that a continuation of such phase fluctuations to zero temperature that are quantum in

[*]maciej.maska@pwr.edu.pl
[†]trivedi.15@osu.edu

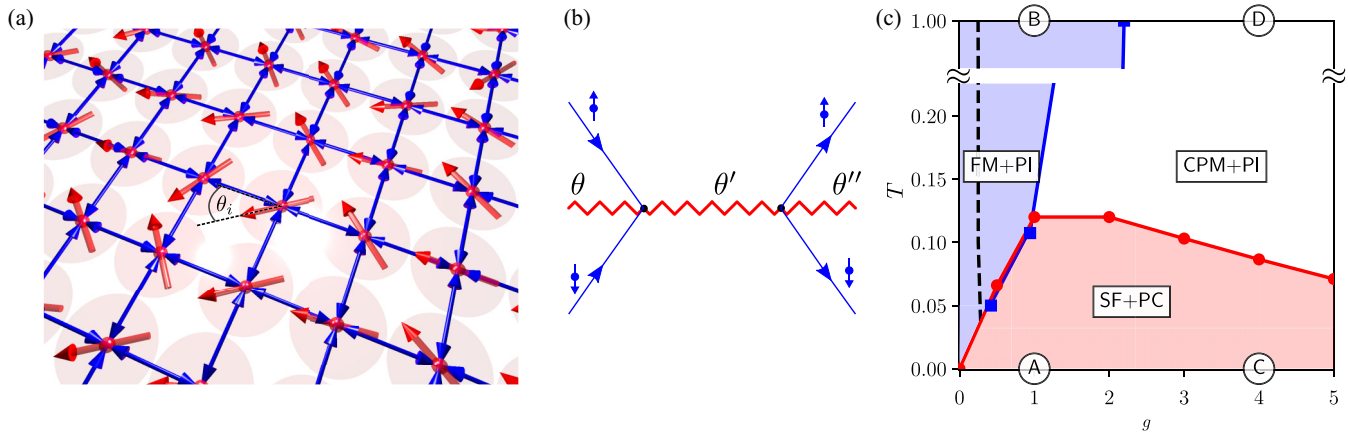

FIG. 1. (a) Illustration of the phase-fermion model: mobile spin-up and spin-down fermions (blue arrows) hop between lattice sites and scatter off localized classical phases (red arrows). (b) Effective phase-mediated interaction between fermions. This process leads to long-range temperature-dependent interactions between the classical phases, and it modifies the spectral properties of the fermions. (c) Phase diagram in the temperature T-coupling g plane: Based on the behavior of phase stiffness Υ, superfluid density ρ_s of fermions, conductivity $\sigma_{\rm dc}$, the inverse participation ratio (IPR), and the fermion spectral gap E_g, we identify the following regions: (i) SF+PC (**S**uper**F**luidity with **P**hase **C**oherence) in which $\rho_s \neq 0$ and $\Upsilon \neq 0$, implying both fermions and phases are coherent. (ii) Fermi metal (FM+PI, **F**ermi **M**etal with **P**hase **I**ncoherence) in which $E_g = 0$, $\sigma_{\rm dc}(T = 0) \neq 0$ and decreasing with temperature, implying that conduction is by single fermions, and the phases are incoherent. In the region to the left of the black dashed line, the IPR indicates extended single-particle wave functions, whereas on the right the single-particle states are weakly localized by the fluctuating phases, though the two-particle states probed by $\sigma_{\rm dc}$ indicate metallic conduction. (iii) **C**ooper **P**air **M**etal (CPM+PI) in which $E_g \neq 0$, so the fermions are gapped out, but $\sigma_{\rm dc}(T = 0) \neq 0$ and decreasing with temperature implying that the conduction is by fermion pairs; the phases are incoherent and disordered. The red line indicates a phase transition from the phase coherent PC to the PI phase determined from the Kosterlitz renormalization-group equations. Letters Ⓐ, Ⓑ, Ⓒ, and Ⓓ mark regimes for which fermionic spectral functions are presented in Fig. 5. The blue line marks the boundary where $E_g = 0$.

nature could drive a Bose metallic phase down to the lowest temperatures.

II. MODEL

We investigate the spectral properties of a model of fermions coupled locally to fluctuating phases, given by the *phase-fermion* (PF) Hamiltonian:

$$H_{\rm PF} = -t \sum_{\langle ij\rangle,\sigma} \hat{c}^\dagger_{i\sigma}\hat{c}_{j\sigma} + g\sum_i (e^{i\theta_i}\hat{c}_{i\uparrow}\hat{c}_{i\downarrow} + \text{H.c.}) - \mu \sum_{i\sigma} \hat{n}^f, \tag{1}$$

where $c^\dagger_{i\sigma}$ ($c_{i\sigma}$) are fermion creation (annihilation) operators, θ_i are classical phases at site i, t is the hopping amplitude of fermions, g is the coupling strength between fermions and phases, and μ controls the number of fermions.

Such an effective model can be obtained from a more microscopic *Bose-fermion* model in which pairs of itinerant fermions with opposite spin can be converted into localized bosons and vice versa, given by

$$H_{\rm BF} = -t \sum_{\langle ij\rangle,\sigma} \hat{c}^\dagger_{i\sigma}\hat{c}_{j\sigma} + \tilde{g}\sum_i (\hat{b}^\dagger_i \hat{c}_{i\uparrow}\hat{c}_{i\downarrow} + \text{H.c.}) - \mu(2\hat{n}^b + \hat{n}^f) + E_B\hat{n}^b, \tag{2}$$

where $\hat{n}^f$ ($\hat{n}^b$) is the density operator for fermions (bosons), μ is the chemical potential that controls the total number of entities, and E_B is the bosonic level. In the limit of a large number of bosons per lattice site, the boson number fluctuations can be neglected and $\hat{b}_i \to \sqrt{n^{\rm b}_i}e^{i\theta_i}$, where n^b_i and θ_i are now classical site-dependent variables. Further, when (i) $E_B = 2\mu$, so that the effective chemical potential for bosons is zero, and (ii) $g \equiv \tilde{g}\sqrt{n^{\rm b}}$, where the amplitude of the boson field is uniform, we obtain the PF effective Hamiltonian (1). We will discuss later realistic systems for which the PF model is a good description.

It is important to note that the PF model does not include a direct interaction between phases θ_i. However, through the interaction with mobile fermions, effective phase-phase interactions get generated. Correspondingly, the properties of the fermions are also affected by their coupling to the phases. Since the local θ_i variables are strongly temperature-dependent, the scattering of fermions off fluctuating phases leads to nontrivial spectral and transport properties of the fermions, most strikingly a temperature-induced BCS-BEC crossover. Figure 1 summarizes the phases that result in the temperature-coupling plane from solving the Hamiltonian in Eq. (1).

III. PHASE SECTOR: EFFECTIVE CLASSICAL HAMILTONIAN

To perform a numerical study of the model in Eq. (1), we integrate out the fermionic degrees of freedom for a given configuration of phases $\vec{\theta} \equiv (\theta_1, \ldots, \theta_N)$, and we obtain an effective action of interacting phases [7]

$$\mathcal{H}(\vec{\theta}) = -\frac{1}{\beta}\sum_n \ln\left[1 + e^{-\beta E_n(\vec{\theta})}\right], \tag{3}$$

where $E_n(\vec{\theta})$ are its single-particle eigenvalues for a given set of θ's and $\beta = 1/k_{\rm B}T$. We address the following questions

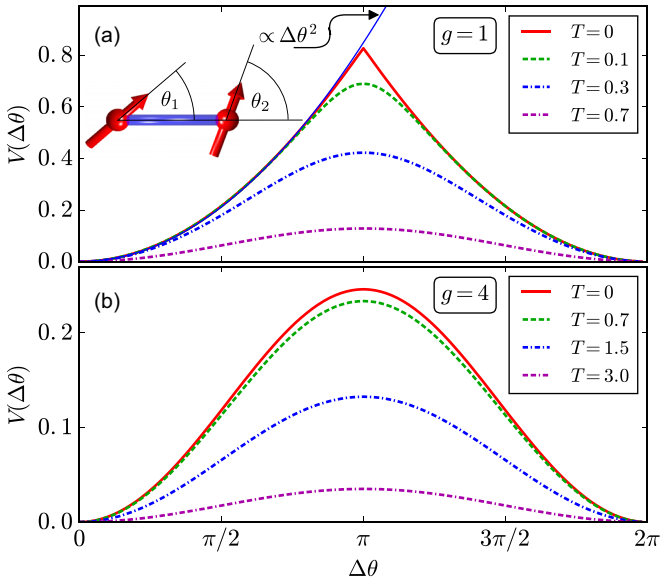

FIG. 2. Phase-phase interaction potential for a two-site PF model given by Eq. (8) for $g = 1$ (a) and $g = 4$ (b). The potentials have been shifted so that $V(0) = 0$. The inset in panel (a) illustrates a two-site PF model: the thick blue line represents fermions coupled to phases θ_1 and θ_2.

about the PF model in the bosonic sector: (i) What are the effective interactions between the phase degrees of freedom generated by integrating out the fermions? (ii) Is there a phase transition from a low-temperature phase-ordered state to a high-temperature phase-disordered state? (iii) Is the transition described by vortex-antivortex unbinding? (iv) How do the phases and phase transitions in the PF model differ from those in the XY model with nearest-neighbor interactions and the associated Berezinskii-Kosterlitz-Thouless (BKT) transition?

A. Insights from a two-site model

The PF model can be analytically solved for a system composed of two sites for which the Hamiltonian is given by [see the inset in Fig. 2(a)]

$$H_{\rm PF}^{\text{2-sites}}(\theta_1,\theta_2) = -t\sum_\sigma (c_{1\sigma}^\dagger c_{2\sigma} + c_{2\sigma}^\dagger c_{1\sigma}) - \mu\sum_\sigma (c_{1\sigma}^\dagger c_{1\sigma} + c_{2\sigma}^\dagger c_{2\sigma}) + g(e^{i\theta_1}c_{1\uparrow}c_{1\downarrow} + e^{i\theta_2}c_{2\uparrow}c_{2\downarrow} + \text{H.c.}) \quad (4)$$

with eigenenergies

$$E_{1,3} = \pm\sqrt{t^2+g^2+\mu^2-2t\,\Xi(\Delta\theta)}, \quad (5)$$

$$E_{2,4} = \pm\sqrt{t^2+g^2+\mu^2+2t\,\Xi(\Delta\theta)}, \quad (6)$$

where $\Delta\theta \equiv \theta_1 - \theta_2$ and $\Xi(\Delta\theta) = \sqrt{\sin^2(\Delta\theta/2)\,g^2+\mu^2}$. The partition function

$$Z = \int d\theta_2 \int d\theta_2 \text{Tr} e^{-\beta H(\theta_1,\theta_2)} = 2\pi \int d\Delta\theta e^{\beta V(\Delta\theta,\beta)}. \quad (7)$$

The effective temperature-dependent interaction between phases θ_1 and θ_2 is given by

$$V(\Delta\theta,\beta) = -\frac{1}{\beta}\sum_{i=1}^{4}\ln\left[1+e^{-\beta E_i(\Delta\theta)}\right] \quad (8)$$

and equals the free energy of the fermionic subsystem. The dependence of the potential on $\Delta\theta$ for $g = 1$ and 4 and at low and high temperatures is depicted in Fig. 2. The limits of the angle-dependent part of V are given by

$$V(\Delta\theta,\beta) \to \begin{cases} A(T)\Delta\theta^2 & \text{for } T\to 0, \\ A(T)\cos(\Delta\theta) & \text{for } T\to\infty, \end{cases} \quad (9)$$

where $\Delta\theta$ is taken modulo 2π. The parameter $A(T) \to 0$ for $T \to \infty$ indicating that the interaction strength decreases with temperature. The difference is pronounced even at small $\Delta\theta$, where in the low-temperature limit the angle-dependent part of $V \propto \cos(\Delta\theta/2)$ in contrast to $V \propto \cos\Delta\theta$ at high temperature. For stronger coupling the difference is much smaller, and for $g = 4$ [Fig. 2(b)] the angle dependence is very well described by $\cos(\Delta\theta)$ at arbitrary temperatures. It can be seen in Fig. 2 that the magnitude of the interaction strongly decreases as the temperature increases.

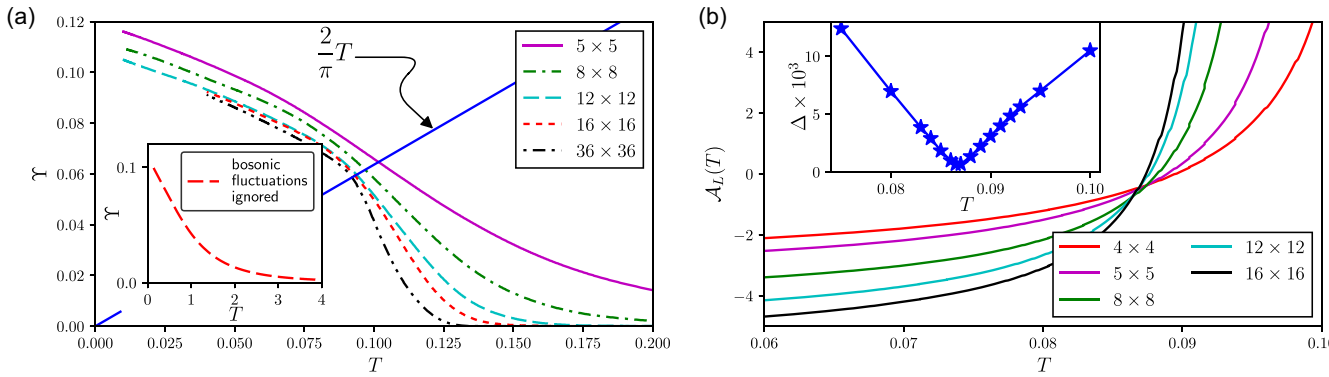

FIG. 3. (a) The temperature dependence of the phase stiffness Υ for $g = 4$ for different system sizes. Υ for the 36×36 system is obtained by using the traveling cluster approximation (TCA) [9]. The straight blue line is the BKT result $\Upsilon = \frac{2}{\pi}T$ for locating the transition. The inset shows Υ for a 16×16 system when only fermions are affected by temperature (see text). (b) The temperature dependence of the left-hand side of Eq. (21) [$\mathcal{A}_L(T)$] for different system sizes. The inset shows the root-mean-square error for fitting Eq. (20) to the MC results.

We can next calculate the number of fermions from the derivative of the thermodynamic potential with respect to μ, which gives

$$N = \sum_{i=1}^{2} \left(1 + \frac{\partial E_i}{\partial \mu} \tanh \frac{\beta E_i}{2}\right). \tag{10}$$

At low temperatures where the phase fluctuations can be neglected, ($\Delta\theta = 0$), we obtain the standard BCS form

$$N = \sum_{i=1}^{2} \left(1 - \frac{\xi_i}{\sqrt{\xi_i^2 + g^2}} \tanh \frac{\beta\sqrt{\xi_i^2 + g^2}}{2}\right), \tag{11}$$

with $\xi_1 = -t - \mu$, $\xi_2 = t - \mu$. For $\mu = 0$, we obtain on average one fermion per lattice site $n^f = 1$. The same holds true also at finite temperatures, where the derivatives in Eq. (10) given by

$$\frac{\partial E_{1,3}}{\partial \mu} = \pm \frac{\mu[t + \Xi(\Delta\theta)]}{\Xi(\Delta\theta)\sqrt{t^2 + \mu^2 + g^2 + 2t\,\Xi(\Delta\theta)}}, \tag{12}$$

$$\frac{\partial E_{2,4}}{\partial \mu} = \pm \frac{\mu[-t + \Xi(\Delta\theta)]}{\Xi(\Delta\theta)\sqrt{t^2 + \mu^2 + g^2 - 2t\,\Xi(\Delta\theta)}}, \tag{13}$$

vanish for $\mu = 0$ and $\Delta\theta \neq 0$. Similarly, $\mu = 0$ gives $n^f = 1$ also for the two-dimensional square lattice if the phases θ_i are fully ordered, i.e., $\theta_i = \theta$ for all lattice sites i. In this case, the system is described by the standard BCS Hamiltonian, and a two-dimensional version of Eq. (11) is valid.

B. Helicity modulus or phase stiffness

The helicity modulus or the phase stiffness Υ can be determined by calculating the free-energy change upon applying a twist to the phases [8], given by

$$\Upsilon = \frac{d^2F(\phi)}{d\phi^2} \approx \frac{F(-\phi) - 2F(0) + F(\phi)}{\phi^2} = 2\,\frac{F(\phi) - F(0)}{\phi^2}. \tag{14}$$

In the MC simulations we fix $\theta_i = 0$ at the left edge of the system and $\theta_i = \phi$ at the right one. Usually $\phi = \pi$ is used in Eq. (14) and the limit $L \to \infty$ is taken. Using this approach, the phase stiffness is expressed by the difference between the free energy for systems with periodic and antiperiodic boundary conditions in the thermodynamic limit [8].

However, since it is much more difficult to get the free energy, we instead transform the phase stiffness expression in terms of the internal energy, according to

$$\frac{1}{2}\frac{d}{d\beta}[\beta\Upsilon(\beta)] = \frac{1}{\phi^2}[\langle\bar{\mathcal{E}}(\phi)\rangle_\beta - \langle\bar{\mathcal{E}}(0)\rangle_\beta], \tag{15}$$

where

$$\langle\bar{\mathcal{E}}(\phi)\rangle_\beta \equiv \frac{1}{Z}\sum_{\{\theta_i\}} \bar{\mathcal{E}}(\vec{\theta}, \phi) e^{-\beta\mathcal{E}(\vec{\theta},\phi)} \tag{16}$$

is determined with the help of the METROPOLIS algorithm, and

$$\bar{\mathcal{E}}(\vec{\theta}, \phi) \equiv \sum_n [\varepsilon_n(\vec{\theta}, \phi) - \mu] f[\varepsilon_n(\vec{\theta}, \phi) - \mu] \tag{17}$$

is the expectation energy of fermions for a given phase configuration $\vec{\theta}$ and twist angle ϕ [$f(\cdots)$ is the Fermi-Dirac distribution function]. Then, the phase stiffness Υ can be calculated as

$$\Upsilon(\beta) = \frac{2}{\beta\phi^2}\int_0^\beta [\langle\bar{\mathcal{E}}(\phi)\rangle_{\beta'} - \langle\bar{\mathcal{E}}(0)\rangle_{\beta'}]d\beta'. \tag{18}$$

Figure 3(a) shows that with increasing system size, Υ becomes steeper, though the systems are still too small to expect any signature of the universal jump in the stiffness at the BKT transition. Another difference between the temperature dependence of the stiffness in the XY and PF models is that in the former case it converges very quickly at low temperature, so that the results even for very small systems are almost the same as in the thermodynamic limit [10]. On the other hand, for the PF model, the convergence is still rather poor at low temperatures and can be attributed to the fact that in the almost ordered state, fermions are itinerant and travel through the entire system so their properties are affected by the size of the system.

Given the stronger size dependence and the inability to observe a jump of the stiffness for bosons interacting via temperature-dependent interactions, we explore a different method to locate T_c. If the stiffness in the PF model follows the Kosterlitz renormalization-group scaling, the stiffness at the BKT transition T_c in the thermodynamic limit should be given by [11]

$$\Upsilon_{L\to\infty}(T_c^-) = \frac{2}{\pi}T_c. \tag{19}$$

The standard method of determining the critical temperature is illustrated in Fig. 3(a). The temperature at which a line representing $\Upsilon(T)$ is crossed by $\frac{2}{\pi}T$ extrapolated to infinite system size should indicate the real T_c. However, since the system size is strongly limited due to the extensive numerical calculations required by exact diagonalization in every MC step, a more precise approach can be used. Namely, to find the critical temperature one can exploit the scaling properties of Υ. The solution of the renormalization-group equations at T_c gives [12]

$$\Upsilon_L = \Upsilon_{L\to\infty}\left[1 + \frac{1}{2}\frac{1}{\ln(L) + C}\right], \tag{20}$$

where C is a constant. Upon inserting $\Upsilon_{L\to\infty} = \frac{2}{\pi}T$ into Eq. (20) we obtain the size dependence of the stiffness Υ. However, Eq. (19) is valid only at $T = T_c$, which implies that when we fit the MC results to the theoretically calculated $\Upsilon(L)$, the fitting errors should be smallest at the critical temperature, thereby allowing a determination of T_c. This is shown in the inset in Fig. 3(b).

We propose a different method below that does not involve a fitting procedure. Combining Eqs. (18), (19), and (20), one finds that at T_c,

$$\left\{\frac{2}{\pi}\int_0^\beta [\langle\bar{\mathcal{E}}(\pi)\rangle_{\beta'} - \langle\bar{\mathcal{E}}(0)\rangle_{\beta'}]d\beta' - 2\right\}^{-1} - \ln(L) = C. \tag{21}$$

Since C does not depend on the system size, if one plots the left-hand side of Eq. (21) [denoted as $\mathcal{A}_L(T)$] as a function of temperature, lines corresponding to different sizes should

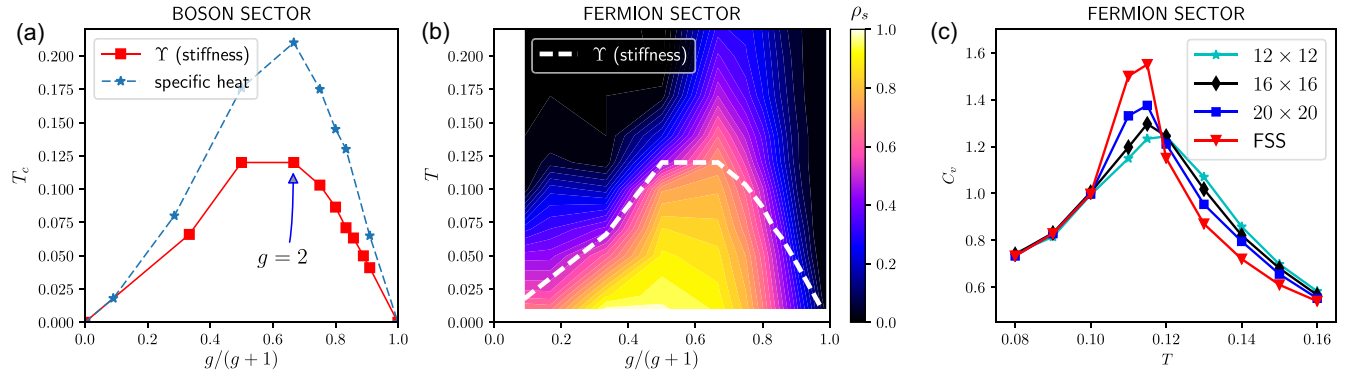

FIG. 4. (a) The BKT critical temperature (red solid line) and the position of the specific-heat maximum (blue dashed line) as a function of $g/(g+1)$ in order to show the weak- and strong-coupling regimes compactly. The specific heat is obtained by using the fluctuation-dissipation theorem. (b) The superfluid density ρ_s (in units of t) of fermions as a function of the coupling g and temperature T. The white dashed line shows the BKT transition [the same as the red line in panel (a)]. (c) Specific heat for $g = 4$ as a function of temperature. The red line (FSS) shows the result of finite-size scaling. In all panels, the lines are only a guide to the eye.

cross at the same point for $T = T_c$. This is presented in Fig. 3(b).

One can notice that the vanishing of the fitting errors [presented in the inset in Fig. 3(b)] and the crossings $\mathcal{A}_L(T)$ for all L in the same point indicate that the itinerant-fermion-mediated interaction between the classical phases leads to a phase transition described by the renormalization-group equations. This means that the phase transition in the PH model is indeed in the BKT universality class.

The phase transition is driven by a softening of the boson phase stiffness and correspondingly also the fermion superfluid stiffness or superfluid density. The inset in Fig. 3(a) demonstrates that the reduction of the boson phase stiffness Υ occurs primarily due to thermal fluctuations of the phases. If we freeze these fluctuations and allow only for thermal fluctuations of the fermions through the broadening of the Fermi function, i.e., if we ignore entropic effects of the phases by choosing phase configurations that minimize the interaction energy rather than the free energy, then we find that Υ [represented by the red dashed line in the inset in Fig. 3(a)] remains finite for temperatures an order of magnitude larger compared to the actual T_c obtained in the correct calculation with thermal fluctuations included in the bosonic sector as well.

By finding the critical temperature for different values of g, one can construct the phase diagram. It is shown in Fig. 4(a), where the solid red and dashed blue lines represent T_c and the position of the specific-heat maximum, respectively. The separation in temperature between the maximum of the specific heat C_v and the BKT transition is much larger for the PF model compared to that in the XY model where the separation is about 10%.

Note that in the strong-coupling regime T_c is inversely proportional to the coupling strength, as is typical for strongly correlated systems.

IV. FERMION SECTOR

We next analyze how the development of phase coherence in the bosonic sector affects the spectral properties of fermions.

A. Spectral function

For a given configuration of the phases $\vec{\theta}$, the real-space fermionic Green function is given by

$$\mathcal{G}(\boldsymbol{R}_i, \boldsymbol{R}_j, z) = \{z - H_{\mathrm{PF}}(\vec{\theta})\}^{-1}_{ij}, \tag{22}$$

where $H_{\mathrm{PF}}(\vec{\theta})$ is given by Eq. (1). We average over configurations $\vec{\theta}$ generated in the MC sampling and integrate out the classical bosonic degrees of freedom. We thus obtain the fermion spectral function from the imaginary part of the Green function:

$$A(\boldsymbol{k}, \omega) = -\frac{1}{\pi}\mathrm{Im}\, \mathcal{G}(\boldsymbol{k}, \omega) \tag{23}$$

and from that the density of states (DOS)

$$N(\omega) = \frac{1}{N}\sum_{\boldsymbol{k}} A(\boldsymbol{k}, \omega), \tag{24}$$

which are shown in Fig. 5.

Even in weak coupling, the system does not behave like a BCS superconductor with a gap magnitude that decreases with temperature and finally closes at T_c. We find in Figs. 5(a), 5(c) and 5(e) for $g = 1$ instead that the gap closes by filling up because the single-particle peaks are broadened with increasing temperature due to the interaction of the fermions with phase fluctuations in the bosonic sector [13]. The spectral function does share some aspects of weak coupling in that the minimum gap occurs at the Fermi energy; the behavior of the spectral functions for smaller g is similar, just with a correspondingly smaller gap.

For strong coupling, $g = 4$ in Figs. 5(b), 5(d) and 5(f), upon increasing T there are two interesting observations: (a) a finite gap persists at high T, and (b) the spectral function looks BEC-like with a minimum gap moving to the Γ point. A similar change in the spectral function has been reported in the attractive Hubbard model on two coupled triangular lattices [14] at $T = 0$ and in the full boson-fermion model within the framework of the bond operator formalism [15]. We report here evidence for a temperature-driven phase transition from a BCS superconductor to a disordered Cooper pair metal. We

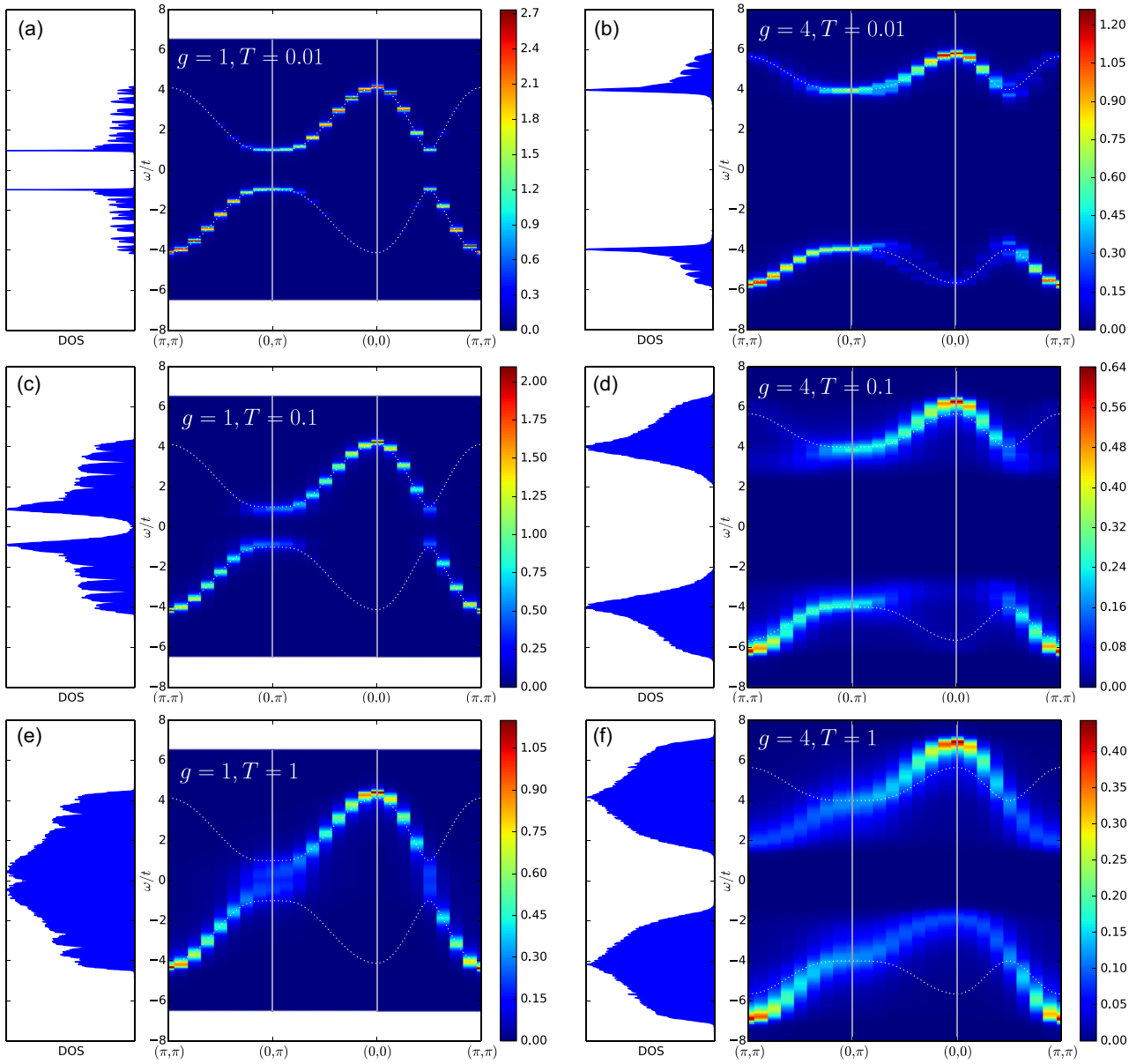

FIG. 5. Densities of states and spectral functions. Left column for $g = 1$: (a) $T = 0.01$, (c) $T = 0.1$, (e) $T = 1$. Right column for $g = 4$: (b) $T = 0.01$, (d) $T = 0.1$, (f) $T = 1$. The white dotted lines show the dispersion of BCS quasiparticles $E_{\boldsymbol{k}} = \pm\sqrt{\varepsilon_{\boldsymbol{k}}^2 + g^2}$. Note that for $g = 4$ the gap minimum moved from the $(0,\ \pi)$ point (consistent with behavior in the BCS regime) to the $(\pi,\ \pi)$ point (consistent with the behavior in the BEC regime) as the temperature increased.

obtain useful insights by solving the PF model on two sites (at momenta $k = 0, \pi$); see Sec. III A.

Essentially, temperature affects the fermionic spectrum primarily via the bosonic phases. At low temperatures, fermions interact with ordered phases and the spectral lines are relatively narrow. At high temperatures, fermions are scattered by the disordered phases that changes their momenta and energies and lead to broadening of the spectral lines. Since the Fermi energy is much higher than the energy scale of the effective interaction between phases mediated by fermions, the broadening due to the Fermi-Dirac distribution function is negligible and does not affect the spectral line shapes. This is also why the observed BCS-BEC crossover can be attributed entirely to scattering off the phases. The behavior closely resembles the disorder-driven BCS-BEC crossover studied previously [16,17]. In our case, however, the disorder is generated dynamically by increasing temperature, as opposed to quenched disorder.

B. Superfluid density

For temperatures up to the BKT transition temperature, fermion-mediated interaction leads to a finite stiffness of the boson phase. At the same time, the phase-fermion interaction present in the Hamiltonian (2) induces pairing among fermions. The pairing amplitude displays a nontrivial temperature dependence across the BCS-BEC crossover. At sufficiently low temperatures, the Cooper pairs become coher-

ent and develop a finite superfluid density given by the Kubo formula [18],

$$\rho_s \equiv \frac{D_s}{\pi} = \langle -k_x \rangle - \Lambda_{xx}(q_x = 0,\ q_y \to 0,\ i\omega = 0) \quad (25)$$

from the difference between the kinetic energy along the x direction (diamagnetic response) and the transverse current-current correlation function (paramagnetic response) given by [19,20]

$$\Lambda_{xx}(\boldsymbol{q}, i\omega_n) = \frac{1}{N}\int_0^{1/T} d\tau\, e^{i\omega_n \tau}\langle \hat{j}_x^p(\boldsymbol{q}, \tau)\hat{j}_x^p(-\boldsymbol{q}, 0)\rangle, \quad (26)$$

where $\hat{j}_x^p(\boldsymbol{q}, \tau)$ is the Fourier transform of the imaginary-time-dependent paramagnetic current in the x direction,

$$\hat{j}_x(\boldsymbol{l}; \tau) = e^{\hat{H}\tau}\left[it \sum_\sigma (\hat{c}^\dagger_{\boldsymbol{l}+\hat{x},\sigma}\hat{c}_{\boldsymbol{l},\sigma} - \hat{c}^\dagger_{\boldsymbol{l},\sigma}\hat{c}_{\boldsymbol{l}+\hat{x},\sigma})\right] e^{-\hat{H}\tau}, \quad (27)$$

and $\omega_n = 2\pi n T$.

$\langle \cdots \rangle$ in Eqs. (25) and (26) denotes a thermal average for a given configuration of the phases $\vec{\theta}$ and an ensemble average over different phase configurations. The former average can be easily calculated as $1/\mathcal{Z}\sum_n \langle n|\cdots|n\rangle$, where $|n\rangle$ is the nth eigenvector of the Hamiltonian $H_{\rm PF}$ for a given configuration of the phases. $\mathcal{Z} = {\rm Tr} e^{-\beta H}$ is the partition function for the same Hamiltonian. The latter average is performed by the MC for the phases.

Figure 4(b) presents the superfluid density ρ_s as a function of interaction g and temperature showing strong reduction of ρ_s along the BKT transition line. We conclude that fermionic superfluidity and bosonic phase coherence occur in the same parameter regimes. This can be understood in the following way: below the BKT transition, the phases are mostly coherent and ordered and do not scatter fermions, which can therefore move coherently. In this regime, the PF model can be accurately described by the mean-field BCS Hamiltonian; see Figs. 5(a) and 5(b). At temperatures above the BKT transition, the phases are strongly fluctuating and incoherent and lead to strong scattering of fermions, resulting in a loss of superfluidity. Given that the effective phase-phase interaction is mediated by fermions and the effective fermion-fermion interaction arises from their coupling to phases, the two subsystems are intimately coupled: coherent fermions enhance boson coherence and vice versa.

C. Single-fermion states

Once long-range phase coherence is lost beyond a critical temperature, what is the fate of fermions? Do they become localized or do they remain itinerant?

We first analyze the nature of single-particle states using the inverse participation ratio, and then we calculate the transport behavior.

The generalized inverse participation ratio [21,22] (IPR) is defined by

$${\rm IPR} = \frac{\sum_{ni}(|u_{ni}|^4 + |v_{ni}|^4)}{\sum_{ni}(|u_{ni}|^2 + |v_{ni}|^2)^2}, \quad (28)$$

where $\vec{\Psi}_n = (u_{n1}, \ldots, u_{nL}, v_{n1}, \ldots, v_{nL})$ is the nth eigenvector of $H_{\rm PF}$. We calculate the IPR on large systems using the traveling cluster approximation [9,23], which tends to zero for delocalized states in the thermodynamic limit and remains finite for localized states.

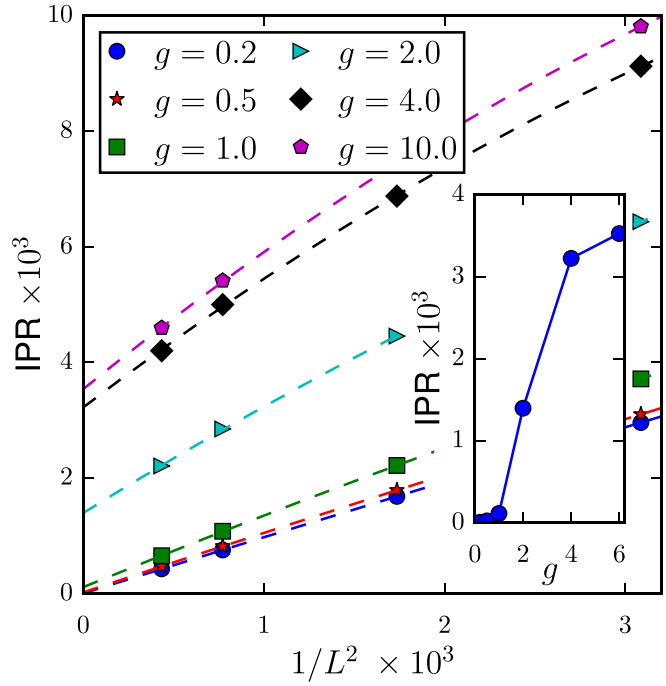

FIG. 6. The IPR calculated at $T = 1$ for different coupling strength. The inset shows the IPR extrapolated to $L = \infty$.

Figure 6 shows the IPR at $T = 1$; in Fig. 1 we mark the region where the IPR vanishes in the $L \to \infty$ limit for a range of temperatures. We find that above the BKT transition, fermions are delocalized only for very weak coupling in the Fermi liquid phase. Stronger coupling between bosons and fermions localizes the single-particle wave functions generating a state with gapless excitations due to their interactions with disordered phases. The transition between localized and delocalized single-particle states is almost independent of

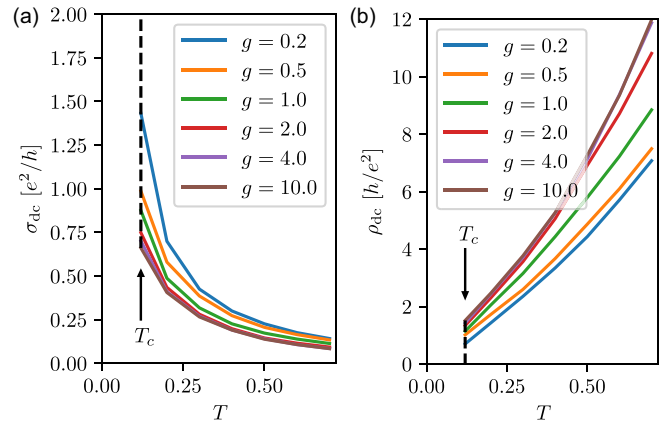

FIG. 7. Temperature dependence of conductivity $\sigma_{\rm dc}$ (a) and resistivity $\rho_{\rm dc} = 1/\sigma_{\rm dc}$ (b) for $T > T_c$ and for different interaction strengths calculated from Eq. (31) in the Cooper-pair-metal (CPM) state. Only data above T_c are presented since for $T < T_c$, $\sigma_{\rm dc} \to \infty$ and $\rho_{\rm dc} \to 0$ in the thermodynamic limit.

temperature. There exists a unitary transformation of the fermionic operators that transfers the bosonic phases to the hopping integral $t \to t \exp[i(\theta_i - \theta_j)/2]$, which introduces a gauge vector potential. It shows that the localization of the single-particle wave functions can be understood also as the localization due to orbital effects of a random magnetic field [24–26]. In the region marked as Cooper pair metal (CPM) in Fig. 1, the single-particle fermionic wave functions are still localized, based on information from IPR, but this region differs from the FM by the presence of a finite gap in the spectrum. The reason we refer to it as metal is because of the transport behavior discussed below. With increasing coupling g, the gap continues to increase, though the superfluid to insulator transition T_{BKT} which is in the BKT universality class shows a nonmonotonic behavior. The overall phase diagram is presented in Fig. 1.

D. Transport

We next discuss the transport properties of the PF model. The optical conductivity $\sigma(\omega)$ is related to the imaginary-time current-current correlation function through

$$\Lambda_{xx}(\boldsymbol{q};\tau) = \int \frac{d\omega}{\pi} \frac{\omega e^{-\tau\omega}}{1-e^{-\beta\omega}} \sigma(\omega), \tag{29}$$

where $\Lambda_{xx}(\boldsymbol{q};\tau)$ is the Fourier transform of the correlation function of the current operator

$$\Lambda_{xx}(\boldsymbol{q};\tau) = \langle \hat{j}_x(\boldsymbol{q};\tau)\hat{j}_x(-\boldsymbol{q};0)\rangle, \tag{30}$$

and the current operator is given by Eq. (27). The way $\langle\cdots\rangle$ in Eq. (30) is calculated is explained below Eq. (27).

While it is possible to calculate $\sigma(\omega)$ by inverting the integral relation (29) with the help of the maximum-entropy method, it can be convenient to estimate the dc conductivity from its low-frequency behavior [27,28]

$$\sigma_{\mathrm{dc}} = \frac{\beta^2}{\pi}\Lambda_{xx}(\boldsymbol{q}=\boldsymbol{0};\tau=\beta/2). \tag{31}$$

The explicit form of $\Lambda_{xx}(\boldsymbol{q};\tau)$ is given by

$$\begin{aligned}
\Lambda_{xx}(\boldsymbol{q};\tau) =& \langle \hat{j}_x(\boldsymbol{q};\tau)\hat{j}_x(-\boldsymbol{q};0)\rangle \\
=& \left\langle e^{\hat{H}\tau}\hat{j}_x(\boldsymbol{q};0)\, e^{-\hat{H}\tau}\hat{j}_x(-\boldsymbol{q};0)\right\rangle \\
=& \frac{1}{\mathcal{Z}}\sum_n \langle n|e^{\hat{H}\tau}\hat{j}_x(\boldsymbol{q};0)e^{-\hat{H}\tau}\hat{j}_x(-\boldsymbol{q};0)|n\rangle e^{-\beta E_n} \\
=& \frac{1}{\mathcal{Z}}\sum_{n,m} \langle n|e^{\hat{H}\tau}\hat{j}_x(\boldsymbol{q};0)e^{-\hat{H}\tau}|m\rangle \\
& \times \langle m|\hat{j}_x(-\boldsymbol{q};0)|n\rangle e^{-\beta E_n} \\
=& \frac{1}{\mathcal{Z}}\sum_{n,m} e^{\tau(E_n-E_m)}\langle n|\hat{j}_x(\boldsymbol{q};0)|m\rangle \\
& \times \langle m|\hat{j}_x(-\boldsymbol{q};0)|n\rangle e^{-\beta E_n}.
\end{aligned} \tag{32}$$

For $\tau = \beta/2$ it takes the following form:

$$\Lambda_{xx}(\boldsymbol{0};\tau=\beta/2) = \frac{1}{\mathcal{Z}}\sum_{n,m} |\langle n|\hat{j}_x(\boldsymbol{0};0)|m\rangle|^2 e^{-\frac{\beta}{2}(E_n+E_m)}. \tag{33}$$

The temperature dependence of conductance σ_{dc} and resistivity $\rho_{\mathrm{dc}} \equiv 1/\sigma_{\mathrm{dc}}$ for different interaction strengths is presented in Fig. 7.

For all values of g the conductance decreases with increasing temperature. What is remarkable is that while the IPR indicates localized single-particle states, the transport is nevertheless metallic. Up to $T \approx 0.25$ we observe a T-linear resistivity, whereas for higher temperatures $\rho_{\mathrm{dc}} \propto T^n$, where $n \approx 1.25$–1.35, which indicates a bad metal-type behavior.

V. DISCUSSIONS AND EXPERIMENTAL IMPLICATIONS

It is remarkable that a simple model like the PF model or the BF model, with no explicit disorder in the Hamiltonian, generates a rich phase diagram with four distinct phases: (i) Fermi metal with both gapped and gapless spectra, (ii) Cooper pair metal with incoherent phases, and (iii) coherent state of phases and fermions with a nonzero phase stiffness and a nonzero superfluid density for the fermions. We arrive at these characterizations of the phases by calculating the IPR to learn about the single-particle wave functions, the single-particle fermionic spectral function for the gap structure in momentum space, the superfluid density for its coherence properties, and conductivity for electric transport properties. We also calculate the helicity modulus to characterize the vortex binding-unbinding BKT transition for the phases.

Kondo lattice and PF model connections: The richness of the PF model extends beyond the specific realization discussed here to other platforms, discussed below. Given the formal correspondence to a model given by Eq. (37), the PF model can describe magnetic atoms deposited on the surface of a superconductor.

Starting with a model of localized spins coupled to spins of itinerant electrons, as in the double-exchange or Kondo-lattice models [29–31], we obtain the spin-fermion Hamiltonian

$$H_0 = -t\sum_{\langle ij\rangle,\sigma} \hat{c}^\dagger_{i\sigma}\hat{c}_{j\sigma} - J\sum_{i\alpha\beta} \boldsymbol{S}_i \cdot c^\dagger_{i\alpha}\boldsymbol{\sigma}_{\alpha\beta}c_{i\beta}, \tag{34}$$

which in the $J/t \to \infty$ limit can be written in a rotated basis as

$$H_0 = \sum_{\langle ij\rangle} t'_{ij}(\hat{\gamma}^\dagger_{i1}\hat{\gamma}_{j1} + \hat{\gamma}^\dagger_{i2}\hat{\gamma}_{j2}) + \mathrm{H.c.}, \tag{35}$$

where t'_{ij} depends on the spins $\boldsymbol{S}_i$ and $\boldsymbol{S}_j$, and $\hat{\gamma}_{i\alpha}$ describes spinless fermions, $\hat{\gamma}_{i\alpha} = \sum_{\beta=1}^{2} A^i_{\alpha\beta}\hat{c}_{i\beta}$, $\alpha = 1, 2$. The effective position-dependent hopping integral can be written in terms of the polar angle (θ_i) and azimuthal angle (ϕ_i) of the spin $\boldsymbol{S}_i$ as $t'_{ij} = -t[\cos\frac{\theta_i}{2}\cos\frac{\theta_j}{2} + \sin\frac{\theta_i}{2}\sin\frac{\theta_j}{2}e^{i(\phi_i-\phi_j)}]$ [32]. The Hamiltonian in Eq. (34) is invariant under the simultaneous global SU(2) rotation of the electron and localized spins, so if the polar angle is fixed by, e.g., the spin-orbit coupling or the pinning effect of an easy-axis magnetic anisotropy energy, without loss of generality it can be set to $\theta_i = \pi/2$. In this case, the effective Hamiltonian is given by

$$H_0 = -t\sum_{\langle ij\rangle} e^{i(\phi_i-\phi_j)}(\hat{\gamma}^\dagger_{i1}\hat{\gamma}_{j1} + \hat{\gamma}^\dagger_{i2}\hat{\gamma}_{j2}) + \mathrm{H.c.} \tag{36}$$

If the localized spins are not coplanar, the magnitude of the hopping integral is site-dependent, $t \to t_{ij}$, but our analysis still applies.

Next, we add singlet pairing to the model,

$$H = H_0 + \sum_i \Delta(c^\dagger_{i\uparrow} c^\dagger_{i\downarrow} + \text{H.c}), \tag{37}$$

which, when rewritten in the $\hat{\gamma}$ basis, gives H in the form

$$H_0 = t \sum_{\langle ij\rangle,\alpha} e^{i(\phi_i - \phi_j)} \hat{\gamma}^\dagger_{i\alpha} \hat{\gamma}_{j\alpha} + \Delta \sum_{i,\alpha} (\hat{\gamma}_{i\alpha} \hat{\gamma}_{i\bar{\alpha}} + \text{H.c.}), \tag{38}$$

where $\bar{1} = 2$ and $\bar{2} = 1$. Introducing new fermionic operators $\hat{d}_{i\uparrow} = e^{i\phi_i/2} \hat{\gamma}_{i1}$ and $\hat{d}_{i\downarrow} = e^{i\phi_i/2} \hat{\gamma}_{i2}$ and defining $\eta_i = \phi_i/2$, we obtain the Hamiltonian

$$H = -t \sum_{\langle ij\rangle,\sigma} \hat{d}^\dagger_{i\sigma} \hat{d}_{j\sigma} + \Delta \sum_i (e^{i\eta_i} \hat{d}_{i\uparrow} \hat{d}_{i\downarrow} + \text{H.c.}), \tag{39}$$

which is formally equivalent to H_{PF} (1). Instead of superfluidity in the bosonic subsystem, this model describes equivalently the spin stiffness in a system in which itinerant electrons are coupled to localized spins. Such systems have recently been studied as possible platforms that host Majorana edge states. Indeed, it has been demonstrated that in one-dimensional systems described by Hamiltonian (37), the RKKY-type interaction can induce a helical magnetic structure, which, when combined with proximity-induced s-wave superconductivity, can drive the system into a topologically nontrivial state [33–42].

In most of the recent studies of this model, it is assumed that the proximity-induced superconductivity in the fermionic sector is not significantly affected by the magnetic structure. Based on our analysis above, it is evident that the interaction works two ways: the itinerant fermions mediate the effective spin-spin interactions, and at the same time scattering from the localized spins strongly affects the properties of the fermions. A self-consistent treatment of the magnetic and superconducting properties is necessary to describe the proximitized magnetic chain.

Graphene with SC islands: Graphene decorated with an array of superconducting islands can also be modeled by an effective PF Hamiltonian (1) [43–48], in which Cooper pairs can tunnel directly between islands whose phases fluctuate with temperature. The BF model suggests that even if the distance between the islands is larger than the range of the superconducting proximity effect, phase ordering in the entire array could occur mediated by the (normal) carriers in graphene that are sensitive to the phases of the superconducting islands.

Electrons scattering off lattice deformations: Electrons interacting with local lattice deformations can be described as an extension of the bipolaronic scenario where strong electron-phonon coupling creates locally bound pairs of small polarons [49]. For intermediate electron-lattice coupling, bipolarons are found to coexist with free-electron pairs [50]. An exchange of charge between wide band electrons and localized pairs gives rise to concentration fluctuations that generate superconductivity in the two subsystems [51]. This idea has been applied to high-temperature superconductivity [52–56], in a generalized form of the plaquette BF model, based on Anderson's RVB scenario [57]. In Ref. [52] it has been demonstrated that in the BF model a pseudogap opens up that evolves into a true gap below the critical temperature. Recently, the boson-fermion model has been adopted to describe resonance superfluids in the BCS-BEC crossover regime [58].

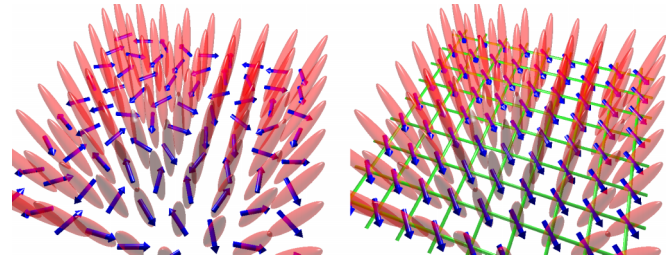

FIG. 8. Square lattice of one-dimensional Bose-Einstein condensate tubes (red) with their phases (blue arrows). The green lines represent the hopping of up and down fermions between sites. The left panel depicts the localization of fermions due to the random fluctuations of the condensate phases. The right panel shows the coherent hopping of fermions once the phases of the BEC tubes become coherent.

Cold-atom platforms: Optical lattices afford a highly tunable platform in which it is possible to take a 3D BEC of tightly bound Cooper pairs (molecules) and break it up into a 2D array of 1D tubes by using an optical lattice applied along two dimensions. Starting from a deep lattice, as the depth is decreased, tunneling between the tubes can drive long-range phase coherence across the entire system. In addition to the bosons, if unpaired fermions are present, they will experience phase fluctuations arising from the tube-BECs. If the lattice potential can localize the molecules but allow the unpaired fermions to tunnel between the BECs, the latter can mediate interboson interactions leading to long-range coherence of the isolated bosons, as shown in Fig. 8.

ACKNOWLEDGMENTS

We would like to acknowledge stimulating discussions with Mohit Randeria. M.M.M. acknowledges support by National Science Centre (Poland) under Grant No. DEC-2018/29/B/ST3/01892, and N.T. acknowledges DOE-Basic Energy Sciences Grant No. DE-FG02-07ER46423. Numerical calculations have been carried out using High Performance Computing resources provided by the Wrocław Centre for Networking and Supercomputing, the Ohio Supercomputer Center, and the Arts and Sciences Technology Services at the Ohio State University.

[1] M. Randeria and E. Taylor, Annu. Rev. Condens. Matter Phys. **5**, 209 (2014).

[2] S. Rinott, K. B. Chashka, A. Ribak, E. D. L. Rienks, A. Taleb-Ibrahimi, P. Le Fevre, F. Bertran, M. Randeria, and A. Kanigel, Sci. Adv. **3**, e1602372 (2017).

[3] Y. Lubashevsky, E. Lahoud, K. Chashka, D. Podolsky, and A. Kanigel, Nat. Phys. **8**, 309 (2012).

[4] W. Ketterle and M. W. Zwierlein, in *Proceedings of the International School of Physics "Enrico Fermi"*, edited by M.

Inguscio, W. Ketterle, and C. Salomon (IOS, Amsterdam, 2008) pp. 95–287.
[5] E. Fradkin, S. A. Kivelson, and J. M. Tranquada, Rev. Mod. Phys. **87**, 457 (2015).
[6] P. W. Anderson, P. A. Lee, M. Randeria, T. M. Rice, N. Trivedi, and F. C. Zhang, J. Phys.: Condens. Matter **16**, R755 (2004).
[7] M. M. Maśka and K. Czajka, Phys. Rev. B **74**, 035109 (2006).
[8] M. E. Fisher, M. N. Barber, and D. Jasnow, Phys. Rev. A **8**, 1111 (1973).
[9] S. Kumar and P. Majumdar, Eur. Phys. J. B **50**, 571 (2006).
[10] Y.-D. Hsieh, Y.-J. Kao, and A. W. Sandvik, J. Stat. Mech.: Theor. Expt. 09 (2013) P09001.
[11] J. M. Kosterlitz, J. Phys. C **7**, 1046 (1974).
[12] H. Weber and P. Minnhagen, Phys. Rev. B **37**, 5986 (1988).
[13] K. Bouadim, Y. L. Loh, M. Randeria, and N. Trivedi, Nat. Phys. **7**, 884 (2011).
[14] Y. L. Loh, M. Randeria, N. Trivedi, C.-C. Chang, and R. Scalettar, Phys. Rev. X **6**, 021029 (2016).
[15] M. Cuoco and J. Ranninger, Phys. Rev. B **74**, 094511 (2006).
[16] S. Tarat and P. Majumdar, Europhys. Lett. **105**, 67002 (2014).
[17] A. Khan, S. Basu, and B. Tanatar, J. Supercond. Novel Magn. **26**, 1891 (2013).
[18] D. J. Scalapino, S. R. White, and S. Zhang, Phys. Rev. B **47**, 7995 (1993).
[19] A. Ghosal, M. Randeria, and N. Trivedi, Phys. Rev. B **65**, 014501 (2001).
[20] T. Das, J.-X. Zhu, and M. J. Graf, Phys. Rev. B **84**, 134510 (2011).
[21] M. Franz, C. Kallin, and A. J. Berlinsky, Phys. Rev. B **54**, R6897 (1996).
[22] M. Franz and Z. Tešanović, Phys. Rev. Lett. **80**, 4763 (1998).
[23] A. Mukherjee, N. D. Patel, C. Bishop, and E. Dagotto, Phys. Rev. E **91**, 063303 (2015).
[24] A. Furusaki, Phys. Rev. Lett. **82**, 604 (1999).
[25] A. Altland and B. Simons, Nucl. Phys. B **562**, 445 (1999).
[26] L. Schweitzer and P. Markoš, Physica E **40**, 1335 (2008).
[27] N. Trivedi, R. T. Scalettar, and M. Randeria, Phys. Rev. B **54**, R3756(R) (1996).
[28] N. Trivedi and M. Randeria, Phys. Rev. Lett. **75**, 312 (1995).
[29] S. Kumar and P. Majumdar, Eur. Phys. J. B **46**, 315 (2005).
[30] P. Sanyal and P. Majumdar, Phys. Rev. B **80**, 054411 (2009).
[31] J. L. Alonso, L. A. Fernández, F. Guinea, F. Lesmes, and V. Martín-Mayor, Phys. Rev. B **67**, 214423 (2003).
[32] J. Alonso, L. Fernández, F. Guinea, V. Laliena, and V. Martín-Mayor, Nucl. Phys. B **596**, 587 (2001).
[33] T.-P. Choy, J. M. Edge, A. R. Akhmerov, and C. W. J. Beenakker, Phys. Rev. B **84**, 195442 (2011).
[34] I. Martin and A. F. Morpurgo, Phys. Rev. B **85**, 144505 (2012).
[35] M. Kjaergaard, K. Wölms, and K. Flensberg, Phys. Rev. B **85**, 020503(R) (2012).
[36] S. Nadj-Perge, I. K. Drozdov, B. A. Bernevig, and A. Yazdani, Phys. Rev. B **88**, 020407(R) (2013).
[37] B. Braunecker and P. Simon, Phys. Rev. Lett. **111**, 147202 (2013).
[38] F. Pientka, L. I. Glazman, and F. von Oppen, Phys. Rev. B **88**, 155420 (2013).
[39] J. Klinovaja, P. Stano, A. Yazdani, and D. Loss, Phys. Rev. Lett. **111**, 186805 (2013).
[40] M. M. Vazifeh and M. Franz, Phys. Rev. Lett. **111**, 206802 (2013).
[41] I. Reis, D. J. J. Marchand, and M. Franz, Phys. Rev. B **90**, 085124 (2014).
[42] A. Gorczyca-Goraj, T. Domański, and M. M. Maśka, Phys. Rev. B **99**, 235430 (2019).
[43] B. M. Kessler, I. M. C. O. Girit, A. Zettl, and V. Bouchiat, Phys. Rev. Lett. **104**, 047001 (2010).
[44] Z. Han, A. Allain, H. Arjmandi-Tash, K. Tikhonov, M. Feigel'man, B. Sacepe, and V. Bouchiat, Nat. Phys. **10**, 380 (2014).
[45] S. Eley, S. Gopalakrishnan, P. M. Goldbart, and N. Mason, Nat. Phys. **8**, 59 (2012).
[46] M. Feigel'man, M. Skvortsov, and K. Tikhonov, Solid State Commun. **149**, 1101 (2009), recent Progress in Graphene Studies.
[47] Y. Sun, H. Xiao, M. Zhang, Z. Xue, Y. Mei, X. Xie, T. Hu, Z. Di, and X. Wang, Nat. Commun. **9**, 2159 (2018).
[48] F. Mancarella, J. Fransson, and A. Balatsky, Supercond. Sci. Technol. **29**, 054004 (2016).
[49] A. Alexandrov and J. Ranninger, Phys. Rev. B **23**, 1796 (1981).
[50] J. Ranninger and S. Robaszkiewicz, Physica B **135**, 468 (1985).
[51] J. Ranninger, R. Micnas, and S. Robaszkiewicz, Ann. Phys. Fr. **13**, 455 (1988).
[52] J. Ranninger, J. M. Robin, and M. Eschrig, Phys. Rev. Lett. **74**, 4027 (1995).
[53] R. Friedberg and T. D. Lee, Phys. Rev. B **40**, 6745 (1989).
[54] V. B. Geshkenbein, L. B. Ioffe, and A. I. Larkin, Phys. Rev. B **55**, 3173 (1997).
[55] T. Domański, M. M. Maśka, and M. Mierzejewski, Phys. Rev. B **67**, 134507 (2003).
[56] M. M. Maśka and M. Mierzejewski, Phys. Rev. B **64**, 064501 (2001).
[57] E. Altman and A. Auerbach, Phys. Rev. B **65**, 104508 (2002).
[58] Y.-i. Shin, C. H. Schunck, A. Schirotzek, and W. Ketterle, Nature (London) **451**, 689 (2008).